Enhanced Backscatter Fibers for Sensing in Telecom Networks

Paul S. Westbrook ⬤, Tristan Kremp ⬤, Benyuan Zhu ⬤, Wing Ko, Zhou Shi, and Kenneth S. Feder

(Invited Paper)

Abstract—We discuss the application of enhanced backscattering fiber in telecom networks. Such fibers can greatly increase the potential of telecom networks to be used as sensors of network health and its surrounding environment. We describe the effects of increased attenuation and multipath interference (MPI) observed in such fibers as the fiber length and backscattering enhancement increases. For MPI we apply both a well known, approximate three bounce treatment as well as a full solution using coupled mode equations, and we verify the validity of the approximate solution. Our analysis allows us to obtain a sensor reach as a function of the backscattering enhancement level and apply this to interrogation schemes for which the minimum required signal power level and the maximum allowable MPI noise level are known. To show that the backscattering enhancement in our fiber does not interfere with telecom signals, we measure the penalty for signals propagating within and near the enhancement bandwidth in a 10 km length of continuously enhanced backscattering fiber. We find that signals only a few nm away from the enhancement bandwidth can propagate without OSNR penalty.

Index Terms—Fiber sensors, optical fibers.

I. INTRODUCTION

DISTRIBUTED acoustic sensing (DAS) is emerging as an important new tool to monitor large linear assets such as oil and gas facilities [1], [2], [3], security systems [4], rail lines [5] and pipelines [6]. It has also been shown that DAS can be used to transform telecom networks into distributed sensors that can detect disturbances near a transmission line such as traffic, construction, or even earthquakes [7], [8], [9]. This powerful technology has the potential to provide significant information about the health of telecom networks as well as the infrastructure in which they are employed. DAS has been enabled by the development of coherent OTDR interrogators [10], [11], [12]. Coherent OTDR measures the distributed backscattering of an optical pulse propagating through long lengths of optical fibers just as the conventional OTDR techniques commonly used to assess telecom networks. However, coherent OTDR systems employ narrow linewidth, low phase noise lasers as the input to the OTDR pulse carving optics. Additional phase and amplitude modulation of the sources allows these interrogators to eliminate various fading artifacts and give a robust signal output. Acoustic signals act to change the optical path along the fiber due to the compression of the silica matrix from the acoustic wave as it impinges on the fiber. This compression of the glass matrix makes the optical path length along the fiber vary from one OTDR pulse to the next. The comparison of successive traces can then be used to record acoustic wave propagation along the length of the fiber. Typical spatial resolution is a few meters and the acoustic frequency range is typically from mHz up to kHz.

A critical limitation of such systems is that they rely on Rayleigh backscattering to generate the coherent OTDR trace. In typical low loss fibers, Rayleigh backscattering is of the order -73 dB per meter of fiber. This weak signal limits various DAS parameters such as spatial resolution, acoustic signal-to-noise ratio (SNR), system reach and frequency response. It has recently been shown that both the optical and acoustic SNR can be increased by more than an order of magnitude through the use of enhanced scattering fibers [13], [14], [15]. Such fibers exhibit a spatially continuous quasi-Rayleigh backscattering over a well defined bandwidth and can have background attenuations below 0.5 dB/km. Enhanced scattering fibers have been shown to completely restore the DAS signal even after attenuation from more than 40 km of fiber [13], [16]. The use of arrays of discrete reflectors with lengths from a few meters to a few kilometers has also been simulated and demonstrated in coherent OTDR systems [17], [18], [19], [20]. We have recently reported on the impact of enhanced backscatter in fiber telecom systems, including the effects of cross talk and attenuation in long fibers [21].

While past demonstrations have used at most a few km of enhanced scattering fiber, there have been no demonstrations over the longer lengths of continuously enhanced scattering fiber suitable for use in telecom applications, typically 10 km or more. Moreover, the effect of such enhanced backscattering on telecom signals has also not been discussed to date, leaving open the question of whether enhanced scattering fibers could carry telecom signals.

Here we go beyond our previous work [21] to address questions about the performance of enhanced scattering fibers in telecom networks. Optical fiber telecommunication differs from applications such as oil field monitoring in several ways. Firstly, the fiber lengths in telecom can be much longer than those in

oil field seismic monitoring, which are typically only a few kilometers long and benefit from very large signal enhancements over the sensitive portion of the fiber. When considering telecom links that can be in excess of 40 km, the effects of both fiber attenuation and multipath interference (MPI) or signal cross talk may have to be taken into consideration. It is also important to consider whether an entire span requires enhanced scattering or whether enhanced scattering fiber is better suited to limited regions of a span where the DAS signal is very low. For instance, in passive optical networks (PONs), there is large attenuation at the optical splitters, but the structures of interest in sensing applications are often located after the splitter [22]. Also, the concept of reach in a distributed sensor system is not the same as in optical fiber communications. In telecommunications, the reach of a system is determined by the signal integrity at the end of the span. However, in distributed sensing, signal is acquired within the fiber span, and it is therefore important to consider the signal enhancement over the entire length of the fiber. As we will discuss in this paper, the primary benefit of enhanced scattering fibers is in increasing the SNR over long fiber spans, rather than greatly increasing the length over which distributed sensing can occur. Thus, even if the enhanced fiber has higher attenuation, it can provide a greater sensing signal over the entire fiber length.

While there have been demonstrations of enhanced scattering fibers, there are no reports of the effect of such enhanced scattering on telecom signals. And while some DAS applications are geared toward the use of dark fiber that carries no signals, it is of interest to understand how DAS can be used in a fiber that is carrying live traffic at the same time. When such a fiber also has enhanced backscattering, then it is necessary to understand the effect of the enhanced backscattering on telecom signals. It is well known that MPI noise can arise from the effect of double Rayleigh backscattering in fiber telecom systems [23], [24], [25]. In fibers with continuously enhanced backscattering, such effects are expected to increase with increasing Rayleigh-like backscatter enhancement. To mitigate such effects, the enhanced backscattering can be confined to a certain range of wavelengths [13]. Telecom signals may then be propagated outside of this scattering bandwidth. However, while the reflectivity of the fiber appears to be similar to Rayleigh scattering outside of such a scattering bandwidth, testing of actual telecom signals has not previously been carried out. Moreover, the OSNR penalty associated with signals that propagate within the scattering bandwidth has also not been measured.

In this paper, we first describe the effects of attenuation and MPI on DAS in long lengths of fiber that exhibit enhanced scattering over their entire length. We aim to do this without reference to a specific DAS interrogation scheme, so we choose measures of the signal degradation due to attenuation and MPI that refer only to the input and output electric fields. We define a system reach for each effect, and we show that these have opposite dependence on the level of backscattering enhancement in the fiber.

In order to characterize the effect of long lengths of enhanced backscattering fiber in telecom systems, we measure the signal propagation over a link that includes 100 km of standard low loss fiber and 10 km of fiber that exhibits enhanced scattering over 15 nm in the C band. We measure the OSNR (Optical Signal

to Noise Ratio) penalty for signals with carrier wavelengths both inside this enhanced scattering bandwidth and outside the scattering bandwidth. We find an OSNR penalty of up to 6.7 dB when the backscatter is approximately 24 dB above Rayleigh backscattering. However, we find that the OSNR penalty is negligible when the carrier wavelength is at least 1 nm outside of the 10 dB scattering bandwidth. Our results indicate that enhanced scattering fibers may be suitable for transmission of telecom signals if the enhanced backscattering is confined to a well defined bandwidth.

II. ATTENUATION IN ENHANCED SCATTERING FIBERS

In this section we consider the effect of fiber attenuation on enhanced scattering fiber. We consider first the backscattered signal power from a single reflection at location z, which is given by

$$P_{\text{signal}}(z) = P_{\text{in}}\rho_e \Delta z e^{-2\alpha_e z}, \tag{1}$$

where P_{in} is the input power, ρ_e is the reflectivity per unit length, Δz is the length of fiber giving rise to the backscatter, and α_e is the fiber attenuation per unit length. To understand the effect of a backscatter enhancement, we normalize the signal to the back reflected power at $z = 0$. In the case where the bare fiber exhibits only Rayleigh scattering, we have

$$P_R(0) = P_{\text{in}}\rho_R \Delta z, \tag{2}$$

where ρ_R is the back reflection per unit length for Rayleigh scattering. More generally for bare fibers that have additional scattering losses beyond Rayleigh scattering, ρ_R is simply the backscattering per unit length of the bare fiber before any treatments to increase backscattering. While enhanced scattering fiber has $\rho_e \geq \rho_R$, the following derivations do not explicitly require this inequality. Note that since Rayleigh scattering arises from a coherent sum of individual scatters with uncorrelated phases, the average power of the Rayleigh backscattering scales with the length of fiber that backscatters. Writing the signal power relative to Rayleigh scattering in dB form, we have:

$$
\begin{aligned}
P_{\text{signal,dB}}(z) &:= 10\log_{10}\frac{P_{\text{signal}}(z)}{P_R(0)} \\
&= 10\log_{10}\frac{P_{\text{in}}\rho_e \Delta z e^{-2\alpha_e z}}{P_{\text{in}}\rho_R \Delta z} \\
&= 10\log_{10}\frac{\rho_e e^{-2\alpha_e z}}{\rho_R} \\
&= R_{e,\text{dB}} - 2\alpha_{e,\text{dB}}z, \tag{3}
\end{aligned}
$$

where $\alpha_{e,\text{dB}} = 10\log_{10}(e)\alpha_e$, which is the fiber attenuation in dB per unit length, and $R_{e,\text{dB}} = 10\log_{10}\frac{\rho_e}{\rho_R}$ is the backscatter per unit length relative to the bare fiber scattering, which is typically dominated by Rayleigh scattering in low loss fibers used in telecom systems. Therefore, we have $R_{e,\text{dB}} = 0$ dB if there is only Rayleigh scattering, i.e., $\rho_e = \rho_R$. We note that in a fiber with enhanced scattering, α_e typically increases as ρ_e is increased, and a figure of merit may be used to compare an enhanced scattering fiber with standard fiber [13]. The relationship between α_e and ρ_e can depend on the approach used to increase backscattering and is still a subject of research.
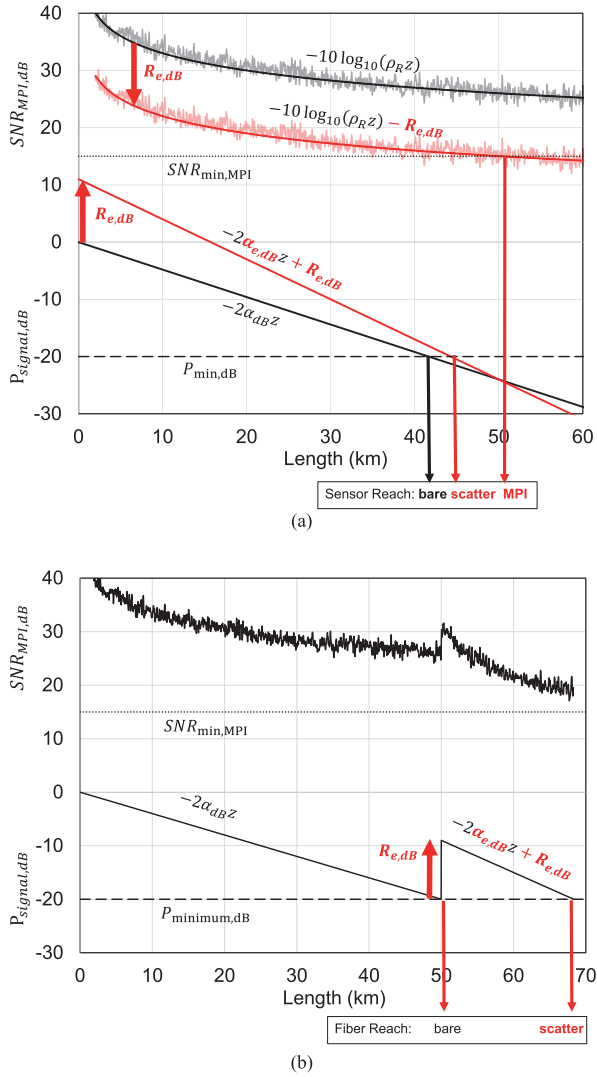
Fig. 1. (a) Illustration of the effect of MPI and attenuation in enhanced scattering fibers. $R_{\text{e,dB}} = 11$ dB is the enhanced reflection over the bare fiber backscattering and is indicated by the red arrows. Black curves are for the bare fiber and red curves are for the enhanced scattering fiber. The bare fiber and enhanced fiber attenuations are taken to be $\alpha_{\text{dB}} = 0.24$ dB/km and $\alpha_{\text{e,dB}} = 0.35$ dB/km, respectively. MPI computations for the simple three bounce model (with $\eta = 1$) are given by the solid line. The full coupled mode solution averaged over 75m is shown by the noisy curves and indicates good agreement with the simple model. (b) Extension of sensor reach of bare fiber with $\alpha_{\text{dB}} = 0.2$ dB/km using enhanced fiber with $R_{\text{e,dB}} = 11$ dB and $\alpha_{\text{e,dB}} = 0.3$ dB/km. The upper noisy curve is the MPI SNR computed with the coupled mode equation model, and the lower curve (piecewise linear) is the signal power $P_{\text{signal}}(z)$.

From (3), it is possible to obtain the maximum reach of the sensor

$$z_{\text{reach,attenuation}} = \frac{R_{\text{e,dB}} - P_{\text{min,dB}}}{2\alpha_{\text{e,dB}}}, \quad (4)$$

where $P_{\text{min,dB}}$ is the minimum signal power level required for effective DAS measurements and depends on Δz. An example is shown at the bottom of Fig. 1(a). As shown in Fig. 1(b), it is also possible to compute the extension of reach when adding an enhanced scattering fiber to an existing fiber of length

$z_{\text{reach,attenuation}}$:

$$z_{\text{reach extension}} = \frac{R_{\text{e,dB}}}{2\alpha_{\text{e,dB}}}. \quad (5)$$

III. MULTIPATH INTERFERENCE IN ENHANCED SCATTERING FIBERS

The other length limitation is due to MPI or cross talk in the fiber arising from multiple reflections before the position z. As the enhancement increases, the MPI increases, degrading the DAS signal quality. The effect of MPI has been considered for many fiber arrays with discrete reflectors, including reflective splices [26], fiber loop mirrors [27], and discrete Bragg gratings [28], [29]. We treat our continuously enhanced scattering fiber as a set of discrete reflectors. Our model is shown in Fig. 2, which depicts a set of N discrete reflectors, separated by a distance Δz. MPI will be seen to depend on the total reflectivity of the fiber, so we first compute this quantity and its dependence on the fiber attenuation. The total average single-bounce reflectivity assuming no attenuation and constant reflectivity per unit length at each point, from all of the fiber up to the point z would be

$$R_{\text{total,0}}(z) = \rho z = \rho N \Delta z. \quad (6)$$

We note that in general, the average reflectivity from a fiber of length z is

$$R_{\text{total}}(z) = \int_0^z \rho(z') e^{-2\int_0^{z'} \alpha(z'')dz''} dz', \quad (7)$$

where both the reflectivity per unit length $\rho(z)$ and attenuation $\alpha(z)$ can vary along the fiber. For the case in which the reflectivity per unit length and attenuation are constant along the fiber, we have $R_{\text{total}}(z) = R_{\text{total,0}}(z)\frac{(1-e^{-2\alpha z})}{2\alpha z}$.

In order to obtain a measure of MPI that is independent of a particular type of DAS interrogation scheme, we characterize MPI by computing the ratio of the reflected electric field E_1 in absence of MPI, i.e., the single bounce E-field, to the reflected electric field that arises from multiple bounces, E_{MPI}. Our modeling will provide a relationship between fiber length, scatter enhancement and the average ratio of signal to MPI noise. We compute the effect of MPI in long lengths of fiber with continuous or quasi continuous enhanced backscattering and compare this effect to that of attenuation. We also compare the lowest order MPI estimate with a full solution of this problem and show that for the levels of enhancement applicable to telecommunications fibers, the lowest order approximation is valid.

The lowest order contribution to the MPI arises from three reflections. The relative electric field amplitude from a single bounce at position z is

$$\varepsilon_1(z) = \sqrt{\rho\Delta z}e^{i\phi(z)-\alpha z} = q(z)\Delta z e^{-\alpha z}, \quad (8)$$

where $\varepsilon(z) = \frac{E(z)}{E_{\text{in}}}$, $E_{\text{in}} = \sqrt{P_{\text{in}}}$ is the magnitude of the input E-field, $\phi(z)$ is the relative optical phase of light scattered at the position z, and $q(z) = \sqrt{\rho/\Delta z}e^{i\phi(z)}$ is the complex-valued reflection coefficient. Since all MPI paths arrive by definition at the same time, the magnitude of this term does not affect
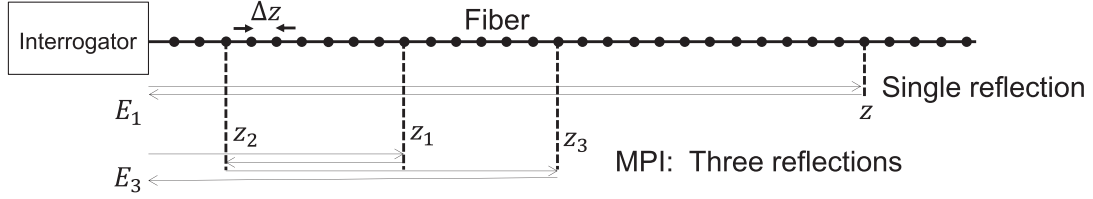
Fig. 2. Model of multipath interference (MPI) in distributed sensing.

the ratio of the single and triple scattering if the attenuation is independent of the position z and we can neglect dispersion (i.e., group velocity equals phase velocity). In other words, the effect of MPI is not affected by the attenuation level when the attenuation is constant.

We model the scattering from position z in the fiber as a discrete sum over $N = z/\Delta z$ discrete scatterers. The three locations for the three-bounce calculation are at $z_j = \Delta z \cdot i_j$ for integer numbers $i_j \leq N$ and $j \in \{1, 2, 3\}$. In the case of a single bounce at location z, the total length of the forward and backward path from 0 to z and back is $z + z = 2z$. Accordingly, for three bounces at locations z_1, z_2 and z_3, the total path length is $z_1 + (z_1 - z_2) + (z_3 - z_2) + z_3 = 2\,(z_1 - z_2 + z_3)$. Both signals interfere if their paths have the same length, i.e., if $z = z_1 - z_2 + z_3$, which is equivalent to $N = i_1 - i_2 + i_3$. Thus, the E-field from all of the three bounce paths can be written as

$$\varepsilon_3\,(z) = (\rho\Delta z)^{\frac{3}{2}} \sum_{i_1=1}^{N} e^{i\phi(z_{i_1})} \sum_{i_2=1}^{i_1} e^{i\left[-\phi(z_{i_2})+\phi(z_{N-i_1+i_2})\right]}. \tag{9}$$

Since the reflection magnitudes are all assumed to be the same, the two sums in (9) can be written as a single sum of $N^2/2$ phasors that describe all possible triple bounce paths. If all these phases were uncorrelated, the expected value $\overline{|\varepsilon_3(z)|}$ of the modulus of (9) would scale as the square root of their number, $\sqrt{N^2/2} = N/\sqrt{2}$, because the modulus of the sum of a circular uniform distribution has a Rayleigh distribution (in the mathematical sense). Taking into account that not all of these $N^2/2$ phases are uncorrelated (e.g., because exchanging z_1 and z_3 in Fig. 2 corresponds to two different triple bounce paths with an identical phasor product), the factor $1/\sqrt{2}$ becomes a factor η of the order of 1 that we will compute more accurately below, so we have with (6)

$$\overline{|\varepsilon_3\,(z)|} = \eta(\rho\Delta z)^{\frac{3}{2}} N = \eta(\rho\Delta z)^{\frac{1}{2}} R_{\text{total},0}\,(z). \tag{10}$$

This expression shows that the MPI from signals with path length $2z$ in the fiber scales with the total power reflected up to z in the absence of attenuation. The SNR defined as the ratio of the single and triple bounce E-fields can with (6) and (10) be expressed as

$$\text{SNR}_{\text{MPI,dB}} = 10\log_{10}\frac{\overline{|\varepsilon_1\,(z)|}}{\overline{|\varepsilon_3\,(z)|}}$$

$$= 10\log_{10}\frac{\sqrt{\rho\Delta z}}{\eta\sqrt{\rho\Delta z}R_{\text{total},0}\,(z)}$$

$$= -10\log_{10}\eta\frac{\rho}{\rho_R}\rho_R z$$

$$= -10\log_{10}\eta\rho_R z - R_{\text{e,dB}}. \tag{11}$$

As indicated by the plot in Fig. 1(a), this E-field ratio decreases by the same amount that the backscattered intensity increases.

As with attenuation, the sensor reach due to MPI can then be related to the minimum tolerable level of MPI which we denote $\text{SNR}_{\text{min,MPI}}$:

$$z_{\text{reach,MPI}} \sim \left(\frac{1}{\rho_R}\right) 10^{-\frac{\text{SNR}_{\text{min,MPI}}+R_{\text{e,dB}}}{10}}. \tag{12}$$

We note that for interrogation methods that are sensitive to the E-field, such as those that interfere the returned signal with a local oscillator, our MPI SNR definition may be appropriate. However, for other interrogation methods that depend on the intensity of the returned signal, our SNR metric may have to be multiplied by a factor of two in order to relate the power (rather than the E-field amplitudes) of the single and multiple bounce E fields.

To justify our above assumption that triple bounce effects dominate MPI while higher orders (5 bounces, 7 bounces, etc.) can be neglected, we now solve the coupled mode equations (CME) [30], [31] that describe the continuous reflections along the fiber. With the reflection coefficient $q(z)$ defined in (8) and with the group velocity v_{g}, the time domain CME for the forward and backward propagating E-field envelopes E_{f} and E_{b}, respectively, are [30, Eq. (7)] [31, Eq. (3)] (the asterisk symbol "$*$" denotes complex conjugation)

$$\frac{1}{v_{\text{g}}}\frac{\partial}{\partial t}\begin{pmatrix} E_{\text{b}}\,(z,t) \\ E_{\text{f}}\,(z,t) \end{pmatrix}$$

$$= \begin{pmatrix} -\frac{\alpha}{2}+\frac{\partial}{\partial z} & -q\,(z) \\ q^*\,(z) & -\frac{\alpha}{2}-\frac{\partial}{\partial z} \end{pmatrix}\begin{pmatrix} E_{\text{b}} \\ E_{\text{f}} \end{pmatrix}. \tag{13}$$

We note that (13) is a consequence of Maxwell's equations under the assumption $|q| \ll 2\pi/\lambda$ at the operating wavelength λ, which is the case for reasonable enhancement levels $R_{\text{e,dB}}$ and discretization grid sizes Δz. We note that by setting $t = 2z/v_{\text{g}}$ and using the notation from above, we have $E(z) = E_{\text{b}}(0, 2z/v_{\text{g}})$ and $\varepsilon(z) = \frac{E(z)}{E_{\text{in}}} = \frac{E_{\text{b}}(0,2z/v_{\text{g}})}{E_{\text{in}}}$.

Separating the off-diagonal (reflection) and on-diagonal (propagation) components in (13), an approximate solution using temporal transfer matrices is (cf. [31], Eq. (9)) with spatial transfer matrices)

$$\begin{pmatrix} E_{\text{b}}\left(z-\Delta z, t+\frac{\Delta z}{v_g}\right) \\ E_{\text{f}}\left(z+\Delta z, t+\frac{\Delta z}{v_g}\right) \end{pmatrix}$$

$$= \mathrm{e}^{-\alpha(z)\Delta z/2} \begin{pmatrix} C(z) & -S(z) \\ S^*(z) & C(z) \end{pmatrix} \begin{pmatrix} E_\mathrm{b}(z,t) \\ E_\mathrm{f}(z,t) \end{pmatrix}, \quad (14)$$

where $C(z) = \cos(|q(z)|\Delta z)$ and $S(z) = \frac{q(z)\sin(|q(z)|\Delta z)}{|q(z)|}$. Equation (14) includes all bidirectional scattering orders, i.e., any integer number of bounces. Even numbers (2, 4, 6,…) of bounces result in forward scattering. In particular, double Rayleigh scattering is subject to two bounces. Accordingly, odd numbers of bounces give rise to backward reflection. In this case, higher reflection orders (3, 5, 7,…) correspond to sensor MPI, while the unperturbed signal is the first reflection order that is subject to the single-bounce CME solution (first Born approximation) that has a vanishing off-diagonal element in the forward direction:

$$\begin{pmatrix} E_\mathrm{b}^{(1)}\left(z-\Delta z, t+\frac{\Delta z}{v_g}\right) \\ E_\mathrm{f}^{(1)}\left(z+\Delta z, t+\frac{\Delta z}{v_g}\right) \end{pmatrix}$$

$$= \mathrm{e}^{-\alpha(z)\Delta z/2} \begin{pmatrix} C(z) & -S(z) \\ 0 & C(z) \end{pmatrix} \begin{pmatrix} E_\mathrm{b}^{(1)}(z,t) \\ E_\mathrm{f}^{(1)}(z,t) \end{pmatrix}. \quad (15)$$

Since it intentionally neglects higher reflection orders, (15) does not conserve power even for vanishing attenuation $\alpha = 0$. In contrast, had we first set the lower left element to zero in the CME (13) and then applied the matrix exponential, the resulting transfer matrix would be closer to unitary (energy-conserving), i.e., the power in higher order reflections would not be correctly disregarded.

The reflected signal $E_\mathrm{b}^{(1)}(0,t)$ at the proximal end $z=0$ of the fiber is a superposition of single bounces that occur along the fiber. In the case of a launched Dirac impulse $E_\mathrm{f}^{(1)}(0,t) \sim \delta(t)$, we have $E_\mathrm{b}^{(1)}(0, 2z/v_\mathrm{g}) \sim q(z)\mathrm{e}^{-\alpha z}$, i.e., the backreflected signal at the proximal fiber end is an attenuated copy of the backscattering coefficient along the fiber. In general, the MPI signal is the difference of the all-bounce solution $E_\mathrm{b}(0,t)$ from (14) and the single-bounce signal $E_\mathrm{b}^{(1)}(0,t)$ from (15):

$$E_\mathrm{b,MPI}(0,t) = E_\mathrm{b}(0,t) - E_\mathrm{b}^{(1)}(0,t). \quad (16)$$

The relative reflected power $P_\mathrm{signal,dB}(z) = 10\log_{10}\frac{|E_\mathrm{b}(0,2z/v_\mathrm{g})|^2}{\rho_\mathrm{R}\Delta z P_\mathrm{in}} = 10\log_{10}\frac{|E(z)|^2}{\rho_\mathrm{R}\Delta z P_\mathrm{in}} = 10\log_{10}\frac{|\varepsilon(z)|^2}{\rho_\mathrm{R}\Delta z}$ is shown in Figs. 3 and 4 for a length of 50 km and values of $\rho_R = 5 \cdot 10^{-5}$/km and $R_\mathrm{e,dB} = 11$ dB. The MPI SNR taken from these plots is also shown in Fig. 1(a). The agreement with the prediction $|\varepsilon_1(z)|^2/\rho_\mathrm{R} = \Delta z \mathrm{e}^{-2\alpha z}\rho/\rho_\mathrm{R}$ from the simple triple bounce result (10) is excellent with the fitting parameter $\eta = 0.9868$ and $\eta = 0.936$, respectively. Figs. 3 and 4 also show the ghost reflections that result from MPI. For times $t > 2N\Delta z/v_\mathrm{group} = 2L/v_\mathrm{group}$, i.e., locations $z > L$, the MPI level decreases because some MPI reflection locations would be beyond the fiber length L as well. Hence, the MPI level is highest at the end $z = L$ of the fiber and may be obtained from the level of the (ghost) reflection just beyond the end of the fiber. This observation is useful in estimating MPI effects from an OTDR trace of a fiber. For instance, if
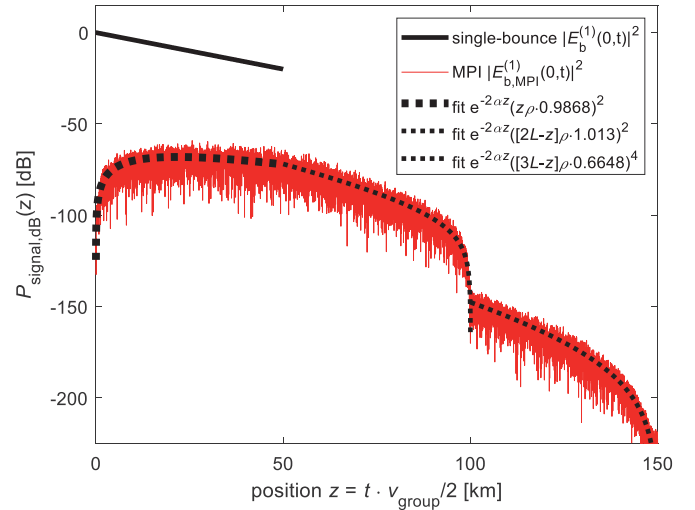

Fig. 3. Reflected signal power $P_\mathrm{signal,dB}(z)$ from (1) for bare fiber of length $L = 50$ km with attenuation $\alpha_\mathrm{dB} = 0.2$ dB/km.
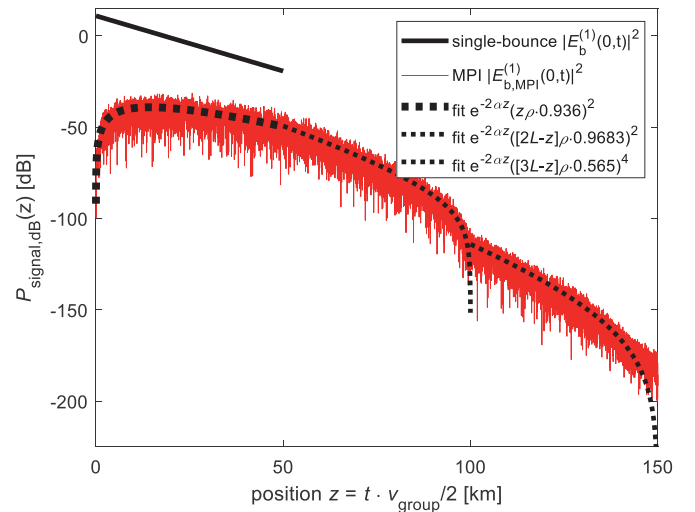

Fig. 4. Reflected signal power $P_\mathrm{signal,dB}(z)$ from (1) for enhanced fiber of length $L = 50$ km with attenuation $\alpha_\mathrm{dB} = 0.3$ dB/km and $R_\mathrm{e,dB} = 11$ dB.

the power of the ghost reflection just beyond the end of the OTDR trace is 20 dB less than the OTDR reflection at the end of the fiber, then the MPI power ratio may be estimated to be 20 dB, and the E-field ratio $\mathrm{SNR}_\mathrm{MPI,dB}$ would be 10 dB. We also indicate in the legends of Figs. 3 and 4 that the higher order ghost reflections can be very well approximated by polynomials in the fiber length. Quantitatively, $P_\mathrm{signal}(z)$ competes with triple bounce MPI $\sim (z\rho\mathrm{e}^{-2\alpha z})^2$ for $0 < z < L$ and $\sim ([2L-z]\rho\mathrm{e}^{-2\alpha z})^2$ for $L < z < 2L$, respectively, and five bounce MPI $\sim ([3L-z]\rho\mathrm{e}^{-2\alpha z})^4$ for $2L < z < 3L$, where the proportionality constants are very close to 1, see the legends of Figs. 3 and 4.
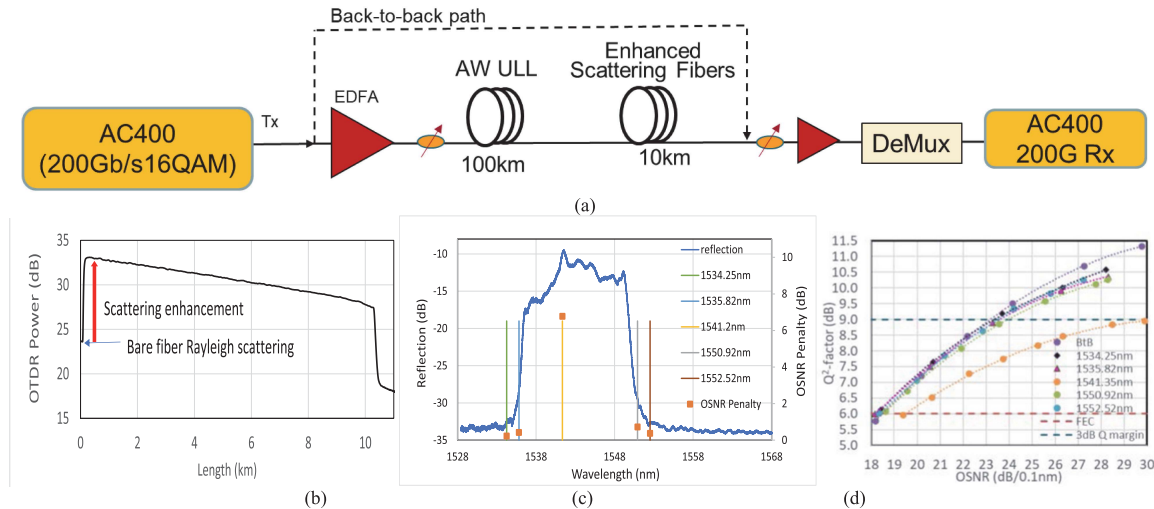
Fig. 5. (a) Telecom test of enhanced scattering fiber. (b) OTDR trace of 10 km of enhanced backscattering fiber. Rayleigh level of bare fiber is evident at fiber length = 0 km. Scattering enhancement is half of the actual value because the y-axis values have been divided by 2 for the OTDR. (c) Optical spectrum of enhanced scattering with lines indicating carrier wavelengths tested in the telecom test bed, as well as the OSNR penalty measured using the carrier wavelengths indicated in the legend. (d) Q^2-factor vs OSNR for back to back (BtB) and for the 110 km link with various signal wavelengths. Error free limit with forward error correction (FEC) threshold and the 3 dB Q margin are shown with dashed lines. OSNR penalty is measured along the 3 dB Q margin line from the BtB curve.

IV. TELECOM TRANSMISSION THROUGH 10 KM OF ENHANCED SCATTERING FIBER

While we have only discussed the sensing properties of enhanced scattering fibers in the previous section, it would also be beneficial if the enhanced sensor fibers could carry telecom data. Fig. 5(c) shows the spectrum of a continuously enhanced scattering fiber of length 10 km. Outside the scattering bandwidth near $\lambda = 1550$ nm, the scattering fiber exhibits backscatter that is very close to that observed in the unprocessed fiber. As a result, the communications capacity of the out-of-band regions are expected to be similar to standard fiber. However to date such measurements have not been performed.

A system demonstration was performed using the experimental fiber link shown in Fig. 5(a). Our link comprised 100 km of Allwave ULL fiber followed by 10 km of enhanced scattering fiber. The enhanced scattering fiber was similar to that in [13]–[16]. The backscatter spectrum is shown in Fig. 5(c). The enhanced scattering $R_{e,dB}$ varies between 15 dB and 24 dB over a bandwidth of approximately 10nm. In a separate OTDR measurement, we measured the attenuation at 1550 nm to be 0.53 dB/km. The Rayleigh level of the bare fiber pigtail is evident at fiber length of 0 km. Note that the level of enhancement must be doubled from the 9 dB increase from the plot. Also note that the OTDR pulse has a large bandwidth close to that of the enhancement bandwidth so the level of enhancement in this plot is an average over that measured in Fig. 5(c). Bit-Error-Ratio (BER) of 200 Gb/s 16QAM channels transmitted over a fiber link as shown in Fig. 5(a) was measured vs. OSNR for different wavelength channels in band where the backscatter was as large as 24 dB over Rayleigh scattering, and out of the band, where the backscattering was much closer to the Rayleigh scattering level. The effect of the enhanced scattering on the quality of digital signal transmission was characterized using the Q^2 factor. Briefly, Q^2 measures the ratio of the average "1" (and "0") values to the range of "1" (and "0") values. A higher Q^2 corresponds to a narrower distribution and a lower BER. The Q^2-factor is related to the system's BER through the complementary error function [32], and is computed from the measured BERs. Fig. 5(d) shows the Q^2-factors vs. OSNR for different wavelength channels transmitted over the total 110 km link as well as the transmitted signal through the back-to-back (BtB) path. For error free transmission, the Q^2-factor must be higher than a certain value defined by the receiver forward error correction (FEC) algorithm. This level is marked by a red dashed line in Fig. 5(d). Practical systems must operate with a higher Q^2-factor (i.e., a lower BER). This Q factor margin level is indicated in Fig. 5(d) by the aqua dashed line. System penalty for a transmitted signal is the additional OSNR, relative to the BtB (ideal) signal, required to reach the Q factor margin level.

The signal penalty values vs wavelength channels are also shown in Fig. 5(c). The penalty at the largest reflectivity was 6.7dB, while the penalty fell to a negligible level when outside the bandwidth of the backscatter. This measurement shows that the introduction of enhanced scattering can be confined to a narrow bandwidth. Signal propagation can still be performed well in the fiber even when the enhancement is present.

V. CONCLUSION

We have described the effects of MPI and attenuation on the performance of backscatter enhanced optical fiber. We derived formulas for the sensor reach due to attenuation and MPI and we showed that an approximate treatment of MPI is sufficient for our enhanced backscattering fiber by comparing it to a full coupled mode equation solution. Our treatments indicate that fibers with an 11 dB enhancement in scattering and 0.35 dB/km attenuation can provide enhanced signals over more than 40 km. In order to show that our fiber can be used in telecom systems, we show that a signal propagating outside the bandwidth of enhanced reflection experiences minimal OSNR penalty due

to the effects of double scattering, while signals within the scattering bandwidth with a backscatter enhancement of 24 dB over Rayleigh scattering experience 6.7 dB of OSNR penalty. Our results indicate that enhanced backscattering fibers can have attenuation and MPI penalties sufficiently low that they be used in fibers with live traffic while still providing enhanced signals for distributed acoustic sensing.

REFERENCES

[1] T. M. Daley et al., "Field testing of fiber-optic distributed acoustic sensing (DAS) for subsurface seismic monitoring," *Leading Edge*, vol. 32, no. 6, pp. 699–706, 2013.

[2] A. Mateeva et al., "Distributed acoustic sensing for reservoir monitoring with vertical seismic profiling," *Geophysical Prospecting*, vol. 62, no. 4, pp. 679–692, 2014.

[3] A. Hartog, B. Frignet, D. Mackie, and M. Clark, "Vertical seismic optical profiling on wireline logging cable," *Geophysical Prospecting*, vol. 62, no. 4, pp. 693–701, Jun. 2014.

[4] A. Owen, G. Duckworth, and J. Worsley, "OptaSense: Fibre optic distributed acoustic sensing for border monitoring," in *Proc. IEEE Eur. Intell. Secur. Inform. Conf.*, 2012, pp. 362–364.

[5] G. Cedilnik, R. Hunt, and G. Lees, "Advances in train and rail monitoring with DAS," in *Proc. 26th Int. Conf. Opt. Fiber Sensors OSA Tech. Dig.*, Sep. 2018, Paper ThE35.

[6] F. Tanimola and D. Hill, "Distributed fibre optic sensors for pipeline protection," *J. Natural Gas Sci. Eng.*, vol. 1, no. 4/5, pp. 134–143, Nov. 2009.

[7] G. A. Wellbrock et al., "First field trial of sensing vehicle speed, density, and road conditions by using fiber carrying high speed data," in *Proc. IEEE Opt. Fiber Commun. Conf. Exhib.*, 2019, pp. 1–3.

[8] N. J. Lindsey et al., "Fiber-optic network observations of earthquake wavefields," *Geophysical Res. Lett.*, vol. 44, no. 23, pp. 11792–11799, Nov. 2017.

[9] P. Jousset et al., "Dynamic strain determination using fibre-optic cables allows imaging of seismological and structural features," *Nature Commun.*, vol. 9, no. 1, pp. 1–11, Jul. 2018.

[10] S. V. Shatalin, V. N. Treschikov, and A. J. Rogers, "Interferometric optical time-domain reflectometry for distributed optical-fiber sensing," *Appl. Opt.*, vol. 37, no. 24, pp. 5600–5604, 1998.

[11] R. Posey, G. A. Johnson, and S. T. Vohra, "Strain sensing based on coherent Rayleigh scattering in an optical fibre," *Electron. Lett.*, vol. 36, no. 20, pp. 1688–1689, Sep. 2000.

[12] T. Parker, S. Shatalin, and M. Farhadiroushan, "Distributed acoustic sensing–a new tool for seismic applications," *First Break*, vol. 32, no. 2, pp. 61–69, Feb. 2014.

[13] P. S. Westbrook et al., "Enhanced optical fiber for distributed acoustic sensing beyond the limits of Rayleigh backscattering," *iScience*, vol. 23, no. 6, Jun. 2020, Art. no. 101137.

[14] N. Lalam, P. S. Westbrook, J. Li, P. Lu, and M. P. Buric, "Phase-sensitive optical time domain reflectometry with Rayleigh enhanced optical fiber," *IEEE Access*, vol. 9, pp. 114428–114434, 2021.

[15] G. A. Wellbrock et al., "Perimeter intrusion detection with backscattering enhanced fiber using telecom cables as sensing backhaul," in *Proc. Opt. Fiber Commun. Conf. Exhib.*, 2022, pp. 1–3.

[16] G. Cedilnik, G. Lees, P. E. Schmidt, S. Herstrøm, and T. Geisler, "Pushing the reach of fiber distributed acoustic sensing to 125 km without the use of amplification," *IEEE Sensors Lett.*, vol. 3, no. 3, Mar. 2019, Art. no. 5000204.

[17] K. Yüksel, J. Jason, E. B. Koal, M. Lopez-Amo, and M. Wuilpart, "An overview of the recent advances in FBG-assisted phase-sensitive OTDR technique and its applications," in *Proc. 22nd Int. Conf. Transparent Opt. Netw.*, 2020, pp. 1–7.

[18] L. D. van Putten et al., "Numerical modelling of a distributed acoustic sensor based on ultra-low loss-enhanced backscattering fibers," *Sensors*, vol. 21, no. 20, Oct. 2021, Art. no. 6869.

[19] M. Wu et al., "Large-scale multiplexed weak reflector array fabricated with a femtosecond laser for a fiber-optic quasi-distributed acoustic sensing system," *Opt. Lett.*, vol. 45, no. 13, pp. 3685–3688, 2020.

[20] H. M. Ogden et al., "Enhanced bandwidth distributed acoustic sensing using a frequency multiplexed pulse train and micro-machined point reflector fiber," *Opt. Lett.*, vol. 47, no. 3, pp. 529–532, 2022.

[21] P. S. Westbrook, K. S. Feder, and T. Kremp, "Enhanced backscatter fibers for sensing in telecom networks," in *Proc. IEEE Opt. Fiber Commun. Conf. Exhib.*, 2022, pp. 01–03.

[22] I. Di Luch, M. Ferrario, P. Boffi, G. Rizzelli, H. Wang, and R. Gaudino, "Demonstration of structural vibration sensing in a deployed PON infrastructure," in *Proc. IEEE 45th Eur. Conf. Opt. Commun.*, 2019, pp. 1–3.

[23] J. L. Gimlett, M. Z. Iqbal, N. K. Cheung, A. Righetti, F. Fontana, and G. Grass, "Observation of equivalent Rayleigh scattering mirrors in light wave systems with optical amplifiers," *IEEE Photonic. Technol. Lett.*, vol. 2, no. 3, pp. 211–213, Mar. 1990.

[24] S. Wu and A. Yariv, "Theoretical and experimental investigation of conversion of phase noise to intensity noise by Rayleigh scattering in optical fibers," *Appl. Phys. Lett.*, vol. 59, pp. 1156–1158, 1991.

[25] P. Wan and J. Conradi, "Impact of double Rayleigh backscatter noise on digital and analog fiber systems," *J. Lightw. Technol.*, vol. 14, no. 3, pp. 288–297, Mar. 1996.

[26] J. P. Dakin, C. A. Wade, and M. Henning, "Novel optical fibre hydrophone array using a single laser source and detector," *Electron. Lett.*, vol. 20, no. 1, pp. 53–54, 1984.

[27] A. D. Kersey, K. L. Dorsey, and A. Dandridge, "Cross talk in a fiber-optic Fabry–Perot sensor array with ring reflectors," *Opt. Lett.*, vol. 14, no. 1, pp. 93–95, Jan. 1989.

[28] D. J. Cooper, T. Coroy, and P. W. Smith, "Time-division multiplexing of large serial fiber-optic Bragg grating sensor arrays," *Appl. Opt.*, vol. 40, no. 16, pp. 2643–2654, 2001.

[29] H. Guo et al., "Crosstalk and ghost gratings in a large-scale weak fiber Bragg grating array," *J. Lightw. Technol.*, vol. 35, no. 10, pp. 2032–2036, May 2017.

[30] R. Feced, M. N. Zervas, and M. A. Muriel, "An efficient inverse scattering algorithm for the design of nonuniform fiber Bragg gratings," *IEEE J. Quantum Electron.*, vol. 35, no. 8, pp. 1105–1115, Aug. 1999.

[31] L. Dong and S. Fortier, "Formulation of time-domain algorithm for fiber Bragg grating simulation and reconstruction," *IEEE J. Quantum Electron.*, vol. 40, no. 8, pp. 1087–1098, Aug. 2004.

[32] N. S. Bergano, F. W. Kerfoot, and C. R. Davidson, "Margin measurements in optical amplifier systems," *IEEE Photon. Technol. Lett.*, vol. 5, no. 3, pp. 304–306, Mar. 1993.

Paul S. Westbrook received the B.S. degree in physics from the University of Michigan, Ann Arbor, MI, USA, and the Ph.D. degree in physics from the Massachusetts Institute of Technology, Cambridge, MA, USA. In 1998, he joined the Optical Fiber Research Department at Bell Laboratories, Murray Hill, NJ, USA. He is currently a Technical Manager with OFS Labs, which was formed after the sale of the Lucent optical fiber business to Furukawa in 2001. He has worked on several optical technologies, including fiber sensors, polarization measurement, fiber lasers, and optical fiber gratings.

Tristan Kremp received the Dipl.-Ing. (M.S.) and Dr.-Ing. (Ph.D.) degrees in electrical engineering from the Karlsruhe Institute of Technology, Karlsruhe, Germany, in 1998 and 2002, respectively, and the Dr.rer.nat. (Ph.D.) degree in mathematics from RWTH Aachen University, Aachen, Germany. From 2002 to 2008, he was with the Institut für Geometrie und Praktische Mathematik, RWTH Aachen University. Since 2008, he has been a Member of Technical Staff with OFS Laboratories. Dr. Kremp was the recipient of multiple awards for his work, which covers a wide range of optical and microwave applications of electromagnetic field simulations, including the design and analysis of hollow core fibers and Bragg gratings, multimode fiber imaging with classical and machine learning methods, mode coupling in waveguides and laser cavities, development of highly efficient wavelet, spectral and quasi-spectral methods for nonlinear optical pulse propagation and multicore fiber splicing, and time domain solutions for scattering problems.

Benyuan Zhu biography not available at the time of publication.

Wing Ko biography not available at the time of publication.

Zhou Shi biography not available at the time of publication.

Kenneth S. Feder biography not available at the time of publication.